EBioMedicine 35 (2018) 270–278

Contents lists available at ScienceDirect

EBioMedicine

journal homepage: www.ebiomedicine.com

EBioMedicine
Published by THE LANCET

Research Paper

Dynamic assessment of tau immunotherapies in the brains of live animals by two-photon imaging

Qian Wu [a], Yan Lin [a], Jiaping Gu [a], Einar M. Sigurdsson [a,b,*]

[a] Department of Neuroscience and Physiology, New York University School of Medicine, 435 East 30th Street, New York, NY 10016, United States
[b] Department of Psychiatry, New York University School of Medicine, 435 East 30th Street, New York, NY 10016, United States

ARTICLE INFO

Article history:
Received 6 March 2018
Received in revised form 3 August 2018
Accepted 14 August 2018
Available online 23 August 2018

Keywords:
Tau protein
Alzheimer's disease
Tauopathy
Antibody
Immunotherapy
Two-photon imaging

ABSTRACT

Our original findings, showing the effectiveness of active and passive tau immunizations in mouse models, have now been confirmed and extended by many groups, with several clinical trials underway in Alzheimer's disease and progressive supranuclear palsy. Here, we report on a unique and sensitive two-photon imaging approach to concurrently study the dynamics of brain and neuronal uptake and clearance of tau antibodies as well as the acute removal of their pathological target in live animals. This in vivo technique is more sensitive to detect clearance of pathological tau protein than western blot tau analysis of brain tissue. In addition to providing an insight into the mechanisms involved, it allows for an efficient in vivo assessment of the therapeutic potential of tau antibodies, and may be applied to related protein misfolding diseases.

1. Introduction

Tau immunotherapies are a promising approach for Alzheimer's disease (AD) and related tauopathies. Our group published the original reports showing the effectiveness of active [1,2] and passive tau immunizations in mouse models [3,4]. These findings have now been confirmed and extended by multiple groups and several clinical trials have already been initiated [5,6]. However, the mechanisms of antibody-mediated clearance of tau aggregates are relatively unclear, although work by us and others has clarified to some extent various pathways that may be involved [5,6].

Two monoclonal antibodies (mAbs) that we have generated against the P-Ser396, 404 tau region, 4E6 and 6B2, have markedly different properties. 4E6 is overall more effective in various culture-, ex vivo- and in vivo models in preventing/reducing tau pathology and associated cognitive impairments, whereas 6B2 or rather its smaller derivatives, may be better suited as a diagnostic imaging marker [7–10]. We showed that the two mAbs are taken up by neurons and microglia and that their neuronal uptake is primarily via clathrin-dependent FcγII/III endocytosis [7–10]. Within tauopathy neurons, these antibodies bind to pathological tau protein primarily within the endosomal/lysosomal system, whereas their uptake/retention is limited in wild-type neurons [7–10].

Advances in imaging techniques now allow direct visualization of brain tissue in live animals by two-photon imaging. Compared to other imaging strategies, two-photon microscopy allows us to monitor the dynamics of mAbs in layers of the cortex (layerII/III) with minimal photo bleaching as reported for amyloid-β (Aβ) antibodies [11]. This permits the study of the time course of the entrance of antibody into the brain following an intravenous injection, its subsequent uptake into neurons as well as its binding to and clearance of tau aggregates in vivo. Monitoring tau clearance can be achieved by co-administration of a pathological tau marker, 1-fluoro-2,5-bis (3-carboxy-4-hydroxystyryl) benzene (FSB). It has been shown to cross the blood-brain-barrier and bind to tau aggregates in the brain as assessed postmortem [12].

In addition to providing such mechanistic insight, our findings show that this technique is a more sensitive way to acutely determine antibody efficacy in clearing pathological tau than by other traditional means such as by western blot analysis. In this regard, it complements

* Corresponding author at: Department of Neuroscience and Physiology, New York University School of Medicine, Science Building, Room 1115, 435 E 30th Street, NY 10016, United States.
E-mail address: einar.sigurdsson@nyumc.org (E.M. Sigurdsson).

https://doi.org/10.1016/j.ebiom.2018.08.041

Research in context

Several antibody therapies targeting the tau protein in Alzheimer's disease are in clinical trials. The live animal imaging approach presented herein provides valuable insight into how these treatments work. In addition, it is more sensitive than standard biochemical measures of brain tissue to detect acute treatment efficacy, which should facilitate identifying candidate tau antibodies for clinical trials. This procedure may also be applied to expeditiously identify potential therapies to clear protein aggregates in related diseases.

cognitive assessment by which we have measured similar acute benefits of the 4E6 antibody [10].

2. Materials and methods

2.1. Animals

The htau model (Jackson Laboratories, stock #004808) [13] was crossed with a model that expresses the PS1 M146L human mutation [14]. The htau mice express unmutated human tau protein on a mouse tau knockout background (mtau KO) and develop tau pathology and tangles with age. The htau X PS1 model on mtau KO background, referred to as htau/PS1, has an earlier onset and more aggressive progression of tau pathology than the htau model. However, since our initial report on this cross [15], its severity has shifted to older age. For all the experiments, female htau/PS1 mice and wild-type (WT) controls of the same gender were at 18–20 months of age. For the study of antibody uptake and clearance (Fig. 1), 4–5 htau/PS1 mice were used per group (IgG1κ, 4E6, or 6B2). Three WT mice per group (4E6 or 6B2) served as controls. For the study of antibody binding to and clearance of pathological tau (Figs. 2, 4-5), 4–6 htau/PS1 mice were used per group (IgG1κ, 4E6, or 6B2). These numbers were based on our past experience with this model, taking into account the data that was acquired sequentially. Analyses of the animal data was randomized and blinded.

All animals were housed at NYU School of Medicine animal facilities and cared for by the veterinary staff in AAALAC-approved facilities. All the procedures were approved by the Institutional Animal Care and Use Committee (IACUC) of the university, and are in accordance with NIH Guidelines, which meet or exceed the ARRIVE guidelines.

2.2. Injected antibodies

Monoclonal antibodies (mAbs) 4E6G7 (hereafter referred to as 4E6) and 6B2G12 (hereafter referred to as 6B2) were purified from our hybridomas by Genscript (Paramus, NJ). IgG1κ (hereafter referred to as IgG1) of the same isotype as the tau mAbs served as control (eBioscience,16–4714). All the antibodies were endotoxin purified by the suppliers and labeled in the laboratory using Alexa Fluor 568 protein labeling kit (Thermo Fisher Scientific, A10238), according to the kit instructions.

2.3. Animal preparation for two-photon imaging

Surgery was performed using aseptic techniques under isoflurane anesthesia (3% for induction, 1.5–2% for surgery). Briefly, the mouse was placed on a heated pad to maintain a body temperature of ~37 °C. The depth of anesthesia was monitored frequently during the surgery. The animal was placed in a stereotaxic frame, incision was made and the skull exposed to reveal the landmarks (bregma, lambda and midline) needed for cranial window. Subsequently, a section of the skull, about 3 mm in diameter, over the right somatosensory cortex was removed.

2.3.1. GFP labeling of neurons

To label neurons, a total of 1–2 μL of AAV5-hSyne-GFP virus (>2×10^{12} genome copies per mL, Penn Vector Core) in an artificial cerebrospinal fluid (ACSF: 125 mM NaCl, 2.5 mM KCl, 2 mM $CaCl_2$, 1 mM $MgCl_2$, 25 mM $NaHCO_3$, 1.25 mM NaH_2PO_4, 25 mM glucose, pH 7.4) was slowly injected by glass micropipette into the cortex (1 mm) over 10–15 min. Then the removed skull section was replaced by a precut #1 round cover glass (Denville Scientific, M0720). Dental cement was used to seal the edges of the cover glass and embed a titanium bar in the dental cement. This bar was used to attach the mouse securely onto the stage of the microscope for imaging. After surgery, the mice were individually housed. Four weeks later, when the window had healed and neuronal GFP expression was robust, the mice received an intravenous mAb injection, followed by two-photon imaging as described below.

2.4. Intravenous injections

2.4.1. Antibodies in neurons

Alexa Fluor 568 labeled IgG1κ, 4E6, or 6B2 were injected (100 μg) into the femoral vein of the htau/PS1 or age-matched wild-type mice with the GFP labeled cortical neurons. Serial two-photon images were obtained at 4 h, 1 day, 4 days, 7 days, and 14 days after injection.

2.4.2. Antibodies bound to pathological tau

In a separate group of mice, 1-fluoro-2,5-bis (3-carboxy-4-hydroxystyryl) benzene (FSB; 0.1%, 300 μL, one injection; Santa Cruz, sc-359,845) was injected into the femoral vein, with or without an immediate follow up injection of 100 μg/200 μL of one of the Alexa Fluor 568 labeled antibodies (IgG1, 4E6, or 6B2) to label brain tau aggregates in vivo. The cranial window and the titanium bar in these mice were prepared in the same manner as described above. The mice were individually housed for 2 weeks after surgery and then FSB and/or antibody were injected followed by serial two-photon imaging at 1 h, 1 day, 4 days, 7 days, and 14 days after injection.

2.5. In vivo two-photon imaging

In vivo imaging was performed on anaesthetized mice (1.0% isoflurane) using Olympus two-photon microscope (FV1000MPE) equipped with a LUMPLFLN 60× water immersion lens (NA1.00) or Olympus two-photon microscope (FVMPE-RS) equipped with a 20× water immersion lens (NA 1.05). The mice were secured under a custom-built head fixation plate. FSB and Alexa 568 labeled antibodies were imaged using 800 nm excitation wavelength and AAV infected neurons were imaged using 920 nm excitation wavelength. Non-descan detector filter cube MRV/G-RXD1 (420–460 nm, EmDM-485) was used for FSB, MRG/R-RXD2 (575–630 nm, EmDM-570) was used for Alexa 568 labeled mAbs and MRG/R-RXD1 (495–540 nm, EmDM-570) was used for neuron-GFP.

Image stacks were analyzed using NIH ImageJ software. The fluorescence intensity of each time point (F) was normalized to Day 1 (F0) when FSB and mAbs had already entered into brain. Neuron/mAbs and FSB/mAbs colocalization coefficient (R) was analyzed using NIH ImageJ software with Colocalization Threshold and Colocalization Test plugins. For neuron and mAbs colocalization, R means Pearson's correlation coefficient for pixels where both 6B2 channel and neuron channel are above their respective threshold within 6B2-positive neurons. For FSB and mAbs colocalization, R means Pearson's correlation coefficient for pixels where both mAb channel and FSB channel are above their respective threshold.

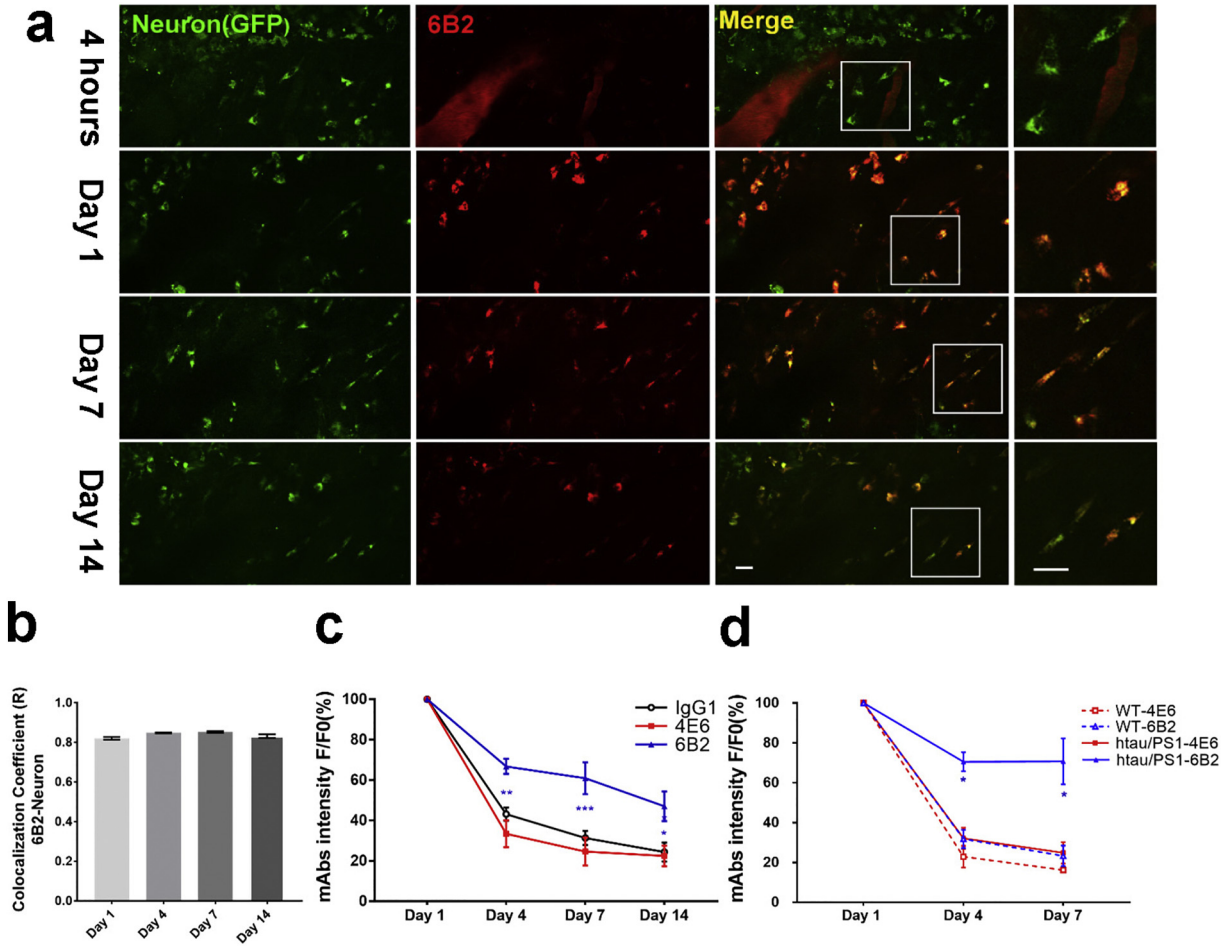

Fig. 1. Two-photon in vivo live imaging reveals that tau mAbs cross the blood-brain-barrier and are primarily detected within neurons. Neuronal 4E6 is cleared faster than 6B2 in htau/PS1 mice and neuronal 6B2 is cleared more slowly in htau/PS1 mice than in WT mice. AAV5-hSyn-eGFP was used to specifically label neurons with GFP in WT or htau/PS1 mice. Alexa 568-IgG1/6B2/4E6 (100 μg) was injected into the femoral vein. Serial two-photon images were then collected from the same brain region over 14 days. a. Representative two-photon image of tau mAb 6B2 brain signal in live htau/PS1 mice. Neuronal (green) intensity remained constant over time, whereas 6B2 (red) intensity decreased during the same period. b. The percentage of 6B2 within neurons remained constant over time although the signal decreased (see a and c). R is Pearson's correlation coefficient for pixels where both 6B2 and neuron channels are above their respective threshold within 6B2-positive neurons. c. Quantitative analysis of antibody neuronal signals during the 14 day imaging period in htau/PS1 mice. $F(3, 35) = 117.8$, $p < .0001$ for time factor and $F(2, 35) = 25.68$, $p < .0001$ for group factor. 6B2 was cleared more slowly from the neurons on Day 4, Day 7 and Day 14 ($p = .0047$, .0004 and .0129, respectively, compared to IgG1 on the same days, two-way ANOVA repeated measures, followed by Tukey's multiple comparisons test). d. Quantitative analysis of neuronal antibody signals during the 7 day imaging period in WT mice, showing for comparison neuronal signals in htau/PS1 mice. $F[2, 24] = 217.2$, $p < .0001$ for time factor and $F[3, 12] = 15.11$, $p = .0002$ for group factor. At 7 days post-injection, 6B2 neuronal signal had decreased to 23% in WT vs. 71% in htau/PS1 mice, compared to Day 1. The 6B2 neuronal signal differed significantly in these two groups on Day 4 ($p = .0342$) and Day 7 ($p = .0196$; Tukey's post-hoc test). Scale bar = 10 μm. F/F0: Ratio of average fluorescence intensity on Day 1 vs. other days. All data are presented as mean ± SEM.*: $p < .05$; **: $p < .01$; ***: $p < .001$.

2.6. Tau extraction and western blots

The left hemisphere of the brain was homogenized in (5 × vol/w) modified RIPA buffer (50 mM Tris-HCl, 150 mM NaCl, 1 mM EDTA, 1% Nonidet P-40, pH 7.4) with protease and phosphatase inhibitors (1 μg/mL of protease inhibitor mixture (cOmplete, Roche), 1 mM NaF, 1 mM Na_3VO_4, 1 mM PMSF, 0.25% sodium deoxycholate). The brain homogenate was centrifuged (20,000 × *g*) for 20 min at 20 °C and supernatants were collected as soluble tau fraction LSS (Low Speed Supernatant). For the sarkosyl insoluble fraction, equal amounts of protein from LSS were mixed with 10% sarkosyl solution to final 1% sarkosyl concentration, and the sample mixed for 30 min at room temperature, then centrifuged at 100,000 × *g* for 1 h at 20 °C. The pellet was then washed with 1% sarkosyl solution and centrifuged again at 100,000 × *g* for 1 h at 20 °C. The sarkosyl pellet (SP) fraction was then air dried for 30 min, mixed with 50 μL of modified O+ buffer (62.5 mM Tris-HCl, 10% glycerol, 5% β-mercaptoethanol, 2.3% SDS, 1 mM EDTA, 1 mM EGTA, 1 mM NaF, 1 mM Na_3VO_4, 1 mM PMSF, and 1 μg/mL of the protease inhibitor mixture). The LSS was eluted with O+ buffer (1:5). LSS and SP in O+ buffer were boiled, and electrophoresed on 12% SDS-PAGE gels and transferred to nitrocellulose membranes. The blots were blocked in Superblock® (Thermo Fisher Scientific), incubated with PHF1 (1:1000, gift from Peter Davies), CP27 (1:500, gift from Peter Davies), GAPDH (1:3000, Cell Signaling Technology, D16H11), AT8 (1:500, ThermoFisher Scientific) AT100 (1:500, ThermoFisher Scientific) and HRP-conjugated anti-Fab secondary antibody (ThermoFisher Scientific), and detected with ECL substrates (ThermoFisher Scientific). Images of immunoreactive bands were acquired by Fuji LAS-4000 imaging system and the bands quantified by MultiGauge software.

2.7. ELISA

To verify that the antibodies were not binding to FSB, the tau labeling dye, IgG1, 4E6 or 6B2 (0.5 μg per well) were coated onto an ELISA plate (Immulon, 2HB, ThermoFisher Scientific) overnight at 4 °C in coating buffer (carbonate-bicarbonate buffer 50 mM, pH = 9.6). Then, FSB (1:10 to 1:100 K) was incubated with the coated plates at room temperature for 3 h. Following three washes in 0.1% TBST, fluorescence

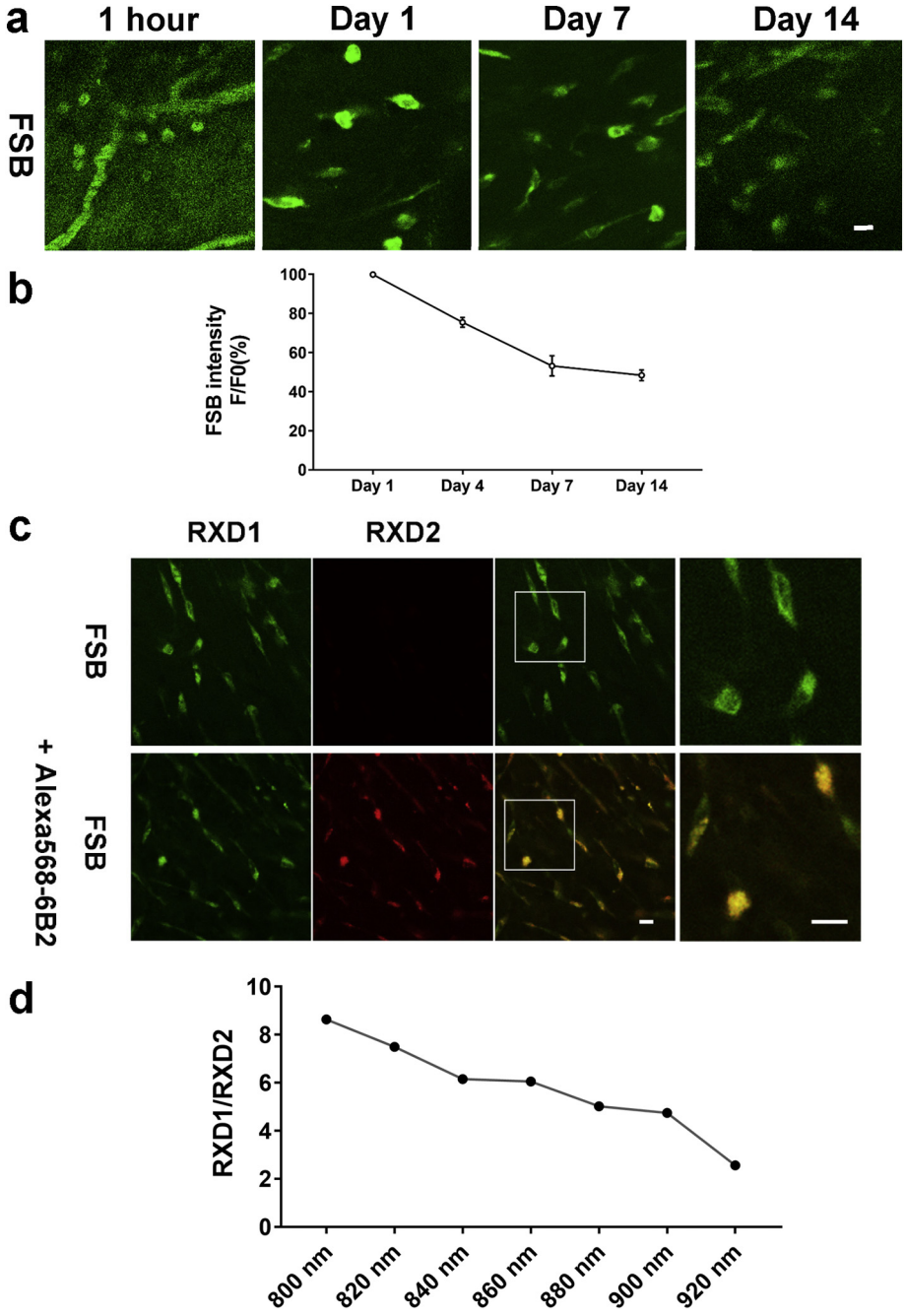

Fig. 2. Characterization of two-photon FSB signal. FSB (0.1%, 300 μL) with or without Alexa568-IgG1/4E6/6B2 (100 μg) was injected into the femoral vein. a. Representative two-photon images of FSB in live htau/PS1 mice without antibody administration on Days 0 (1 h), 1, 7 and 14. b. Quantitative analysis of FSB signal during the 14 day imaging period in htau/PS1 mice that received a single injection of FSB and no antibody. The signal gradually decreases over time. c. Two-photon in vivo images of FSB with or without co-injection of Alexa568-6B2 one day after injection. FSB signal was collected through RXD1 (420–460 nm), and Alexa 568-6B2 signal was collected through RXD2 (575–630 nm) and the signals do not overlap. d. Ratio of RXD1/RXD2 at different excitation wavelength. FSB was injected alone and 800 nm excitation wavelength was selected for later use, because FSB had the highest signal with limited spectral bleed-through at this wavelength. F/F0: Ratio of average FSB fluorescence intensity on Day 1 vs. other days. Scale bar = 10 μm. All data are presented as mean ± SEM.

endpoint signal was detected by BioTek Synergy™ 2 (Biotek Instrument, Inc) with the excitation wavelength 395 nm–445 nm and emission wavelength 475 nm–495 nm. For positive control, wells were loaded with the FSB dilutions immediately before signal detection.

2.8. Immunohistochemistry

After imaging studies, brains were collected for immunohistochemistry assays. Briefly, the mice were perfused transaortically with PBS and the extracted brains were fixed in 4% paraformaldehyde at 4 °C overnight, followed by at least 24 h immersion in 2% DMSO and 20% glycerol in phosphate buffer at 4 °C, and then cryo-sectioned coronally at 40 μm as previously described in detail [16]. FSB and Alexa-568 labeled monoclonal antibodies were directly visualized using a Nikon C-1 confocal microscope. For immunostaining, the brain sections were permeabilized with 0.3% Tween-20 and incubated with respective primary antibodies overnight and secondary antibodies for 1 h at room temperature. Brain FSB signal after its intravenous injection is mostly cleared during standard defatting and rehydration histological processing of mounted tissue sections. Hence, sections were restained with FSB (0.1%) in the same manner as standard Thioflavin S staining [16], to examine its postmortem co-localization with injected 4E6 or PHF1-stained sections.

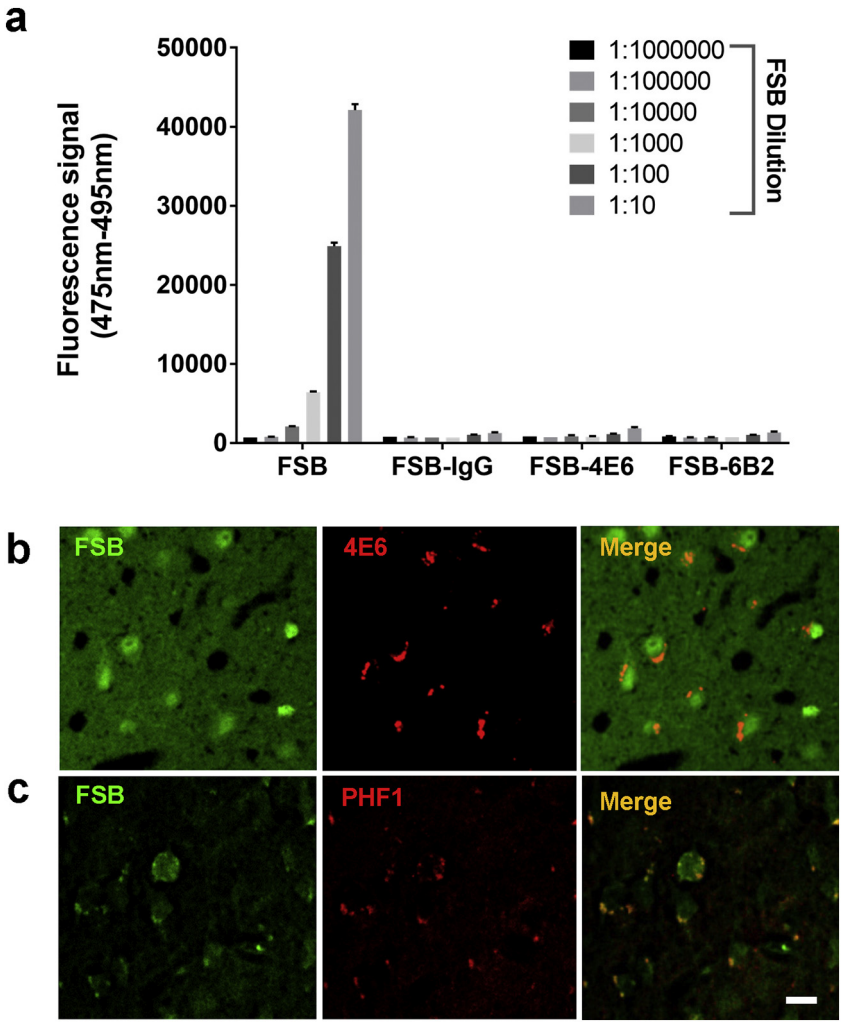

Fig. 3. FSB does not bind to the antibodies, and its staining of histological brain sections reveals colocalization with the injected tau antibody. a. Compared to positive FSB control, the tau antibodies 4E6 and 6B2 or control IgG1 do not bind to FSB on ELISA plates. This indicates that the colocalization of FSB with the antibodies observed in vivo is not due to non-specific interactions. b. After the last imaging session at 7 days, fixed htau/PS1 brain sections from FSB + 4E6 injected htau/PS1 mouse were restained with FSB (green) because it clears during the standard defatting and rehydration procedure. The image shows its partial colocalization with injected Alexa-568 labeled 4E6 (red). c. Staining of fixed htau/PS1 brain sections from an untreated control htau/PS1 mouse shows partial co-localization of FSB (green) with phospho-tau antibody PHF1 (red), indicating that FSB can bind to pathological phospho-tau protein. Scale bar = 10 μm. All data are presented as mean + SEM.

2.9. Statistical analyses

GraphPad Prism 7 was used for statistical analyses. The intensity changes of mAbs and FSB over time were analyzed using two-way ANOVA, repeated measures, with Tukey's post-hoc test. Colocalization and Western blot data was analyzed using one-way ANOVA with Dunnett's post-hoc test. Significance levels were set at $P < .05$. All data are presented as mean ± SEM.

3. Results

3.1. Tau mAbs and control IgG cross the blood-brain barrier and are primarily detected within neurons. Neuronal 4E6 is cleared faster than 6B2 in htau/PS1 mice

To determine blood-brain-barrier (BBB) permeability, neuronal uptake and clearance of tau antibodies in live htau/PS1 tauopathy mice, neurons were GFP tagged by AAV virus infection, and Alexa 568-IgG1 control, Alexa 568-4E6 tau mAb or Alexa 568-6B2 tau mAb (100 μg) were injected into the femoral vein of the tauopathy mice (18–20 months). Two-photon live images were collected at Day 0, 1, 4, 7 and 14 from the same animal. Most of the 6B2 mAb (≥ 95%) was still in the blood vessels 4 h after injection (Fig. 1a). At 24 h (Day 1), 6B2 was primarily found within neurons ($R = 0.78$) and gradually decreased up to 14 days post-injection (Fig. 1b-c). Consistently, about 80% of the antibody was found within neurons, indicating comparable clearance from different cell types / binding sites (Fig. 1b). The distribution of the tau 4E6 mAb and control IgG1 from blood to neurons within the brain followed a similar pattern as for 6B2, although the kinetics differed (Fig. 1c). IgG1, 4E6 and 6B2 were decreased within neurons to 24%, 22% and 47% on Day 14 compared to Day 1. Two-way ANOVA analysis showed significant time and group effects ($F(3, 35) = 117.8$, $p < .0001$ and $F(2, 35) = 25.68$, $p < .0001$, respectively). 6B2 was cleared more slowly on Day 4, Day 7 and Day 14 ($p = .0047$, .0004 and .0129, respectively; Tukey's post-hoc test), compared to IgG1 on the same days [8].

3.2. Neuronal 6B2 signal is cleared more slowly in htau/PS1 mice than in wild-type mice

To explore whether pathological tau levels affect the clearance of mAbs in live mice, Alexa 568-4E6 or Alexa 568-6B2 (100 μg) were separately injected into htau/PS1 mice or wild-type (WT) mice. Changes in

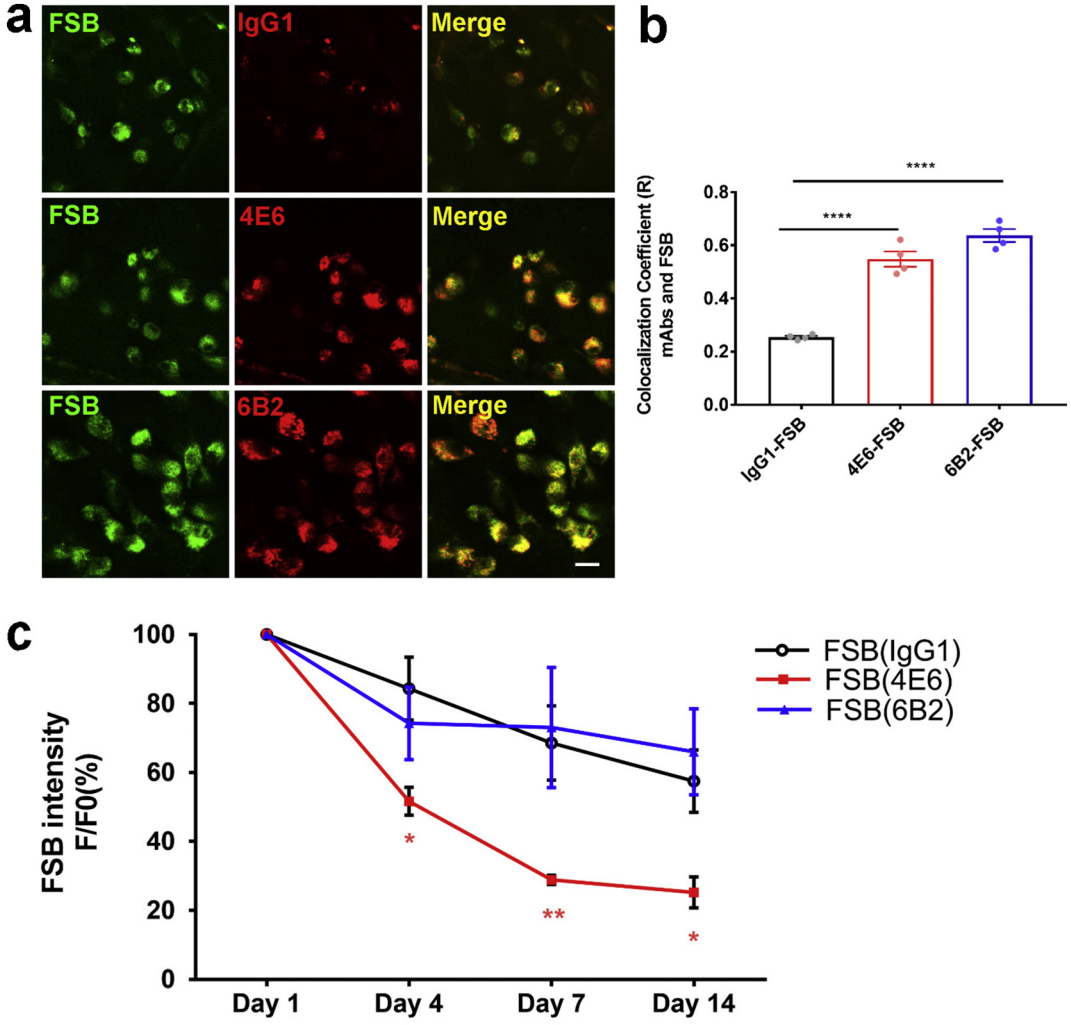

Fig. 4. Two-photon in vivo live imaging of FSB colocalization with tau mAbs and 4E6 is more effective than 6B2 in clearing tau aggregates. FSB (0.1%, 300 μL) with Alexa 568-IgG1/4E6/6B2 (100 μg) were injected into the femoral vein of the htau/PS1 mice. Serial two-photon images were then collected of the same brain region over 14 days and FSB intensity was analyzed. a. Representative two-photon in vivo live images showing excellent co-localization of FSB and tau mAbs 4E6 and 6B2 4 days after their injection. b. Quantification of FSB colocalization with different mAbs. R is Pearson's correlation coefficient for pixels where both mAb and FSB channels are above their respective threshold. $F[2, 9] = 83.16$, $p < .0001$ one-way ANOVA. The tau mAbs 4E6 and 6B2 co-localized more significantly with FSB ($R = 0.55$, $R = 0.64$, respectively, $p < .0001$; Dunnett's post-hoc test), compared to IgG1 ($R = 0.25$). c. FSB intensity in the brain decreased over time, and more with 4E6 than 6B2 or IgG1. $F(3, 35) = 20.56$, $p < .0001$ for time factor and $F(2, 35) = 13.17$, $p < .0001$ for group factor. FSB signal decreased faster when it was co-injected with 4E6 on Day 4, Day 7 and Day 14 ($p = .0246$, .0056 and .0427, respectively), compared to IgG1 on the same day (two-way ANOVA, repeated measures, Tukey's multiple comparisons test). F/F0: Ratio of average fluorescence intensity on Day 1 vs. other days. Scale bar = 10 μm. All data are presented as mean ± SEM. *: $p < .05$; **: $p < .01$; ****, $p < .0001$.

the fluorescence signal were detected by two-photon microscope at Day 1, Day 4, and Day 7. Similar to our findings in htau/PS1 mice (Fig. 1a), most of mAb signal in WT mice was in blood vessels 4 h after mAbs injection, leading to extensive neuronal signal within the brain 24 h after injection (data not shown). In all the groups, mAbs signal decreased over the 7 day imaging period (Fig. 1d). Antibody clearance was comparable in 4E6 injected WT and htau/PS1 mice and 6B2 injected WT mice but was much less in 6B2 injected htau/PS1 mice. Two-way ANOVA analysis showed significant time ($F[2, 24] = 217.2$, $p < .0001$) and group ($F[3, 12] = 15.11$, $p = .0002$) effects. At 7 days post-injection, neuronal 6B2 signal had decreased to 23% in WT vs. 71% in htau/PS1 mice, compared to Day 1. The neuronal 6B2 signal differed significantly in these two groups on Day 4 ($p = .0342$) and Day 7 ($p = .0196$; Tukey's post-hoc test).

3.3. 4E6 and 6B2 colocalize with a tau aggregate dye probe in htau/PS1 mice

To clarify if the antibodies are binding to pathological tau in htau/PS1 mice, 1-fluoro-2,5-bis (3-carboxy-4-hydroxystyryl) benzene (FSB) was used to label tau tangles [12]. FSB (0.1%, 300 μL) with or without Alexa 568-IgG1, 4E6 or 6B2 (100 μg) was injected into the femoral vein of the mice (18–20 months), and live images were collected. FSB images after one i.v. injection were collected at Day 0, Day 1, Day 4, Day 7 and Day 14 (Fig. 2a). FSB appeared to enter the brain parenchyma faster than the antibodies as it was clearly detected outside the vasculature 1 h after the femoral vein injection vs 4 h for the antibodies (Fig. 1a). FSB signal was decreased to 75%, 53% and 48% on Day 4, 7 and 14 compared to Day 1 (Fig. 2b). The optimal excitation wavelength for FSB and Alexa 568 labeled mAbs was found to be at 800 nm, which resulted in the highest signal and limited spectral bleed-through (Fig. 2c-d). To rule out non-specific binding of FSB with the mAbs, different mAbs were coated onto ELISA plate and incubated with different dilution of FSB (1:10 to 1:100 K). Dose-dependent FSB fluorescence signal was detected in FSB positive control group, but FSB did not bind to the mAbs (Fig. 3a). To further clarify FSB binding, its staining of brain sections from mice that had received intravenous injections of labeled 4E6 showed its partial neuronal co-localization with the injected tau antibody (Fig. 3b). FSB binding to phospho-tau was further confirmed by co-staining of brain tissue from untreated animals with PHF1, showing

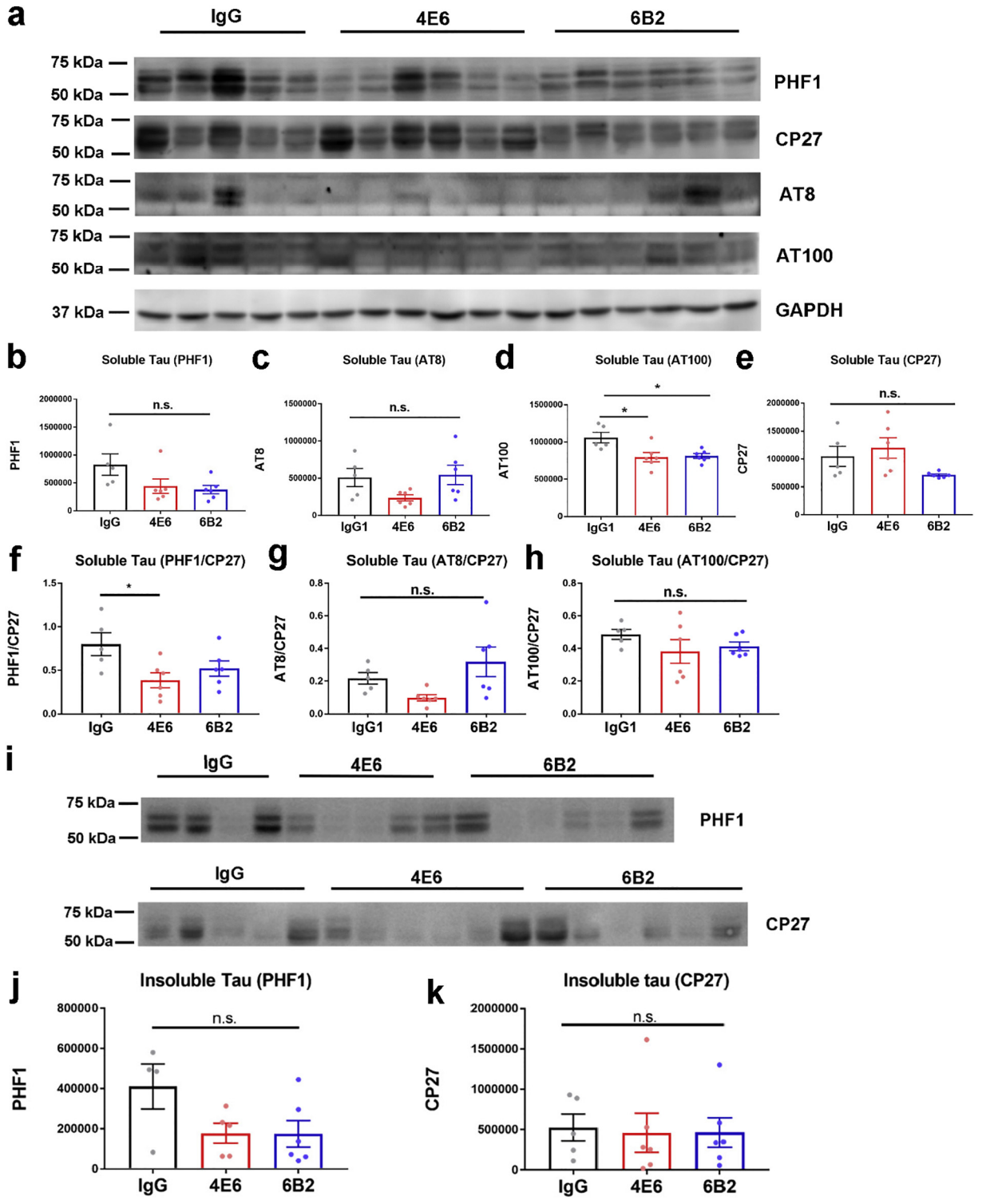

Fig. 5. A single intravenous injection of 4E6 or 6B2 has limited effects on tau pathology as measured by Western blots. a. Western blots for soluble protein fraction stained with PHF1 (phospho-tau), AT8 (phospho-tau), AT100 (phospho-tau), CP27 (human tau) and GAPDH (loading control). b-h. Quantification of protein levels in a. b. Soluble PHF1 level ($F[2, 14] = 3.096$, $p = .0770$). c. Soluble AT8 level ($F[2, 14] = 2.758$, $p = .0977$). d. Soluble AT100 level ($F[2, 14] = 6.349$, $p = .0109$). e. Soluble CP27 level ($F[2, 14] = 3.101$, $p = .0768$). f. Soluble PHF1/CP27 ($F[2, 14] = 4.299$, $p = .035$). g. Soluble AT8/CP27 ($F[2, 14] = 3.609$, $p = .0544$). h. Soluble AT100/CP27 ($F[2, 14] = 1.096$, $p = .3613$). Both 4E6 and 6B2 decreased soluble phospho-tau AT100 levels ($p = .0115$ and 0.0165, respectively; Dunnett's post-hoc test). 4E6, but not 6B2, decreased soluble phospho-tau PHF1/CP27 levels ($p = .0215$; Dunnett's post-hoc test). i. Western blots for insoluble protein fraction stained with PHF1 and CP27. j-k. Quantification of protein levels in i. The single intravenous injection of tau antibodies 4E6 or 6B2 did not alter insoluble tau levels. j. Insoluble PHF1 level ($F[2, 12] = 2.942$, $p = .0913$). k. Insoluble CP27 level ($F[2, 14] = .02948$, $p = .9710$). All data are presented as mean ± SEM. *: $p < .05$.

their partial colocalization (Fig. 3c). One-way ANOVA showed significant group effect on antibody colocalization with FBS in the cortex of the mice when analyzed 4 days post-injection ($F[2, 9] = 83.16$, $p < .0001$). The tau mAbs 4E6 and 6B2 significantly co-localized with FSB ($p < .0001$, Dunnett's post-hoc test; $R = 0.55$, $R = 0.64$, respectively), compared to IgG1 ($R = 0.25$; Fig. 4a-b).

3.4. 4E6 is more effective than 6B2 in clearing tau aggregates

To clarify if the antibodies are promoting clearance of pathological tau, two-photon images were collected after FSB co-injection with IgG1, 4E6 or 6B2 (100 μg) on Day 1, Day 4, Day 7 and Day 14. FSB intensity in the brain decreases over time, and more with 4E6 than 6B2 or control IgG1 (Fig. 4c). Two-way ANOVA analysis showed significant time and group effects ($F(3, 35) = 20.56$, $p < .0001$ and $F(2, 35) = 13.17$, $p < .0001$). FSB signal decreased faster, when it was co-injected with 4E6, on Day 4, Day 7 and Day 14 ($p = .0246$, .0056 and .0427, respectively, compared to IgG1 on the same day, Tukey's post-hoc test). However, FSB injected with 6B2 was cleared at a similar rate as with IgG1. Following imaging on Day 14, the brains were collected for biochemical analysis of tau to determine if these differences in FSB clearance rate were reflected in soluble (Fig. 5a-h) and insoluble tau fractions (Fig. 5i-k). One-way ANOVA analysis showed significant group effect on soluble phospho-tau AT100 and PHF1/CP27 (Fig. 5d, f, AT100, $F[2, 14] = 6.349$, $p = .0109$; PHF1/CP27, $F[2, 14] = 4.299$, $p = .035$). Both 4E6 and 6B2 decreased soluble phospho-tau AT100 levels (Fig. 5d, $p = .0115$ and .0165; Dunnett's post-hoc test). 4E6, but not 6B2, decreased soluble phospho-tau PHF1/CP27 levels (Fig. 5f, $p = .0215$; Dunnett's post-hoc test). There was no significant group effect on insoluble tau level (Fig. 5i-k).

4. Discussion

In this study, we measured and analyzed dynamic changes in fluorescently labeled tau mAbs and in a tau β-sheet dye in live mice by two-photon imaging. We found that the tau mAbs crossed the BBB and were primarily detected within neurons (Fig. 1a-b). One of the tau mAbs, 6B2, was cleared more slowly and to a lesser extent in tauopathy mice than the other tau mAb, 4E6, which was cleared at a similar rate as a control IgG (Fig. 1c). In WT mice, both tau antibodies were cleared at a similar pace and to a comparable degree (Fig. 1d). These clearance differences between the two tau mAbs can be explained by their different binding properties. Although 4E6 and 6B2 were generated to target the same tau peptide P-Ser396, 404 region, 4E6 binds better to soluble tau and 6B2 binds more strongly with insoluble tau [10]. Previously, we identified 6B2 and its scFv derivate as potential imaging ligands to detect tau pathology using an In Vivo Imaging System (IVIS) [9]. The 4E6 tau mAb gives overall less IVIS signal in the same mice than 6B2, based on our preliminary results [17], which fits well with the two-photon findings.

Apart from providing detailed information on the vascular vs cellular distribution of the ligand, which is not possible with the IVIS approach, the two-photon method is much more sensitive. That is as expected because the skull and skin obviously diminish the IVIS signal. With the two-photon technique, we found that most of the mAb signal was in blood vessels 4 h after injection, and approximately 25–50% of the antibody remained in the brain, predominantly within neurons (about 80%) 14 days following the intravenous injection (Fig. 1a-b). In our prior IVIS study, the signal remained relatively stable for a few hours and then gradually subsided over a week back to background values [9]. The key advantage of the IVIS method is its non-invasiveness as a signal can be obtained from an intact animal. However, unlike the two-photon approach, it cannot provide information on the vascular vs cellular distribution of the ligand(s) under study. The large percentage of the antibodies detected within neurons is analogous to our prior report on tau antibody uptake in brain slice culture derived from mouse tauopathy brain [8]. There, about 10% of the tau antibodies added to the brain slice culture were detected within microglia. One would perhaps expect a larger percentage of antibodies within those phagocytic cells, but their clearance of antibody-tau complexes is likely more efficient than in neurons, resulting in an underestimate of antibody uptake into microglia. In addition, most of pathological tau resides within neurons. That fact, coupled with their slower clearance of antibody-tau complexes explains the high percentage of neuronal tau antibodies.

Co-injection of the tau β-sheet dye FSB and tau antibodies clearly showed that these markers associate within neurons, where most of pathological tau is found in these animals (Fig. 4a-b). Such intraneuronal association of tau antibody with pathological tau in vivo fits prior reports from us and others, showing with different methodologies in postmortem tissue that tau antibodies enter the brain and neurons, in which they bind to pathological tau [2,7–10,18–20]. Similar intraneuronal binding of antibodies to other protein aggregates has been reported by various laboratories [21–24]. FSB has previously been shown to label brain tau aggregates upon postmortem examination after peripheral injection [12], and not to give a two-photon signal in wild-type mice [25]. Another β-sheet dye that labels various amyloids, including tau and Aβ, has previously been shown to label tau tangles in mice as detected by two-photon imaging following topical application [26], as unlike FSB, it does not readily cross the blood brain barrier. Not all tau antibodies are readily taken up into neurons [27–29] as such uptake is likely charge-dependent [6].

FSB co-localizes well with the tau antibodies within brain neurons in the two-photon images when both are injected (Fig. 4a). However, only a partial co-localization is seen when brain sections are stained with FSB following 4E6 antibody injection (Fig. 3b). Such direct staining showed more binding than can be expected with two-photon imaging. Furthermore, 4E6 binding to tau may diminish further FSB binding to that particular site. For these two reasons, overlap between FSB and tau antibody is only partial in the histological sections (Fig. 3b). Gradual binding to tau of FSB and tau antibody following an intravenous injection can be expected to result in a more mosaic pattern of binding and therefore better colocalization as observed. In addition, the 4E6 signal in the histological sections is more condensed/vesicle-like than following two-photon imaging. This may be explained by the different time period from injection to imaging in these images (7 days in Fig. 3b vs 4 days in Fig. 4a). With time, 4E6 becomes more condensed within neurons, presumably as it goes down the endosomal/lysosomal pathway as we have previously shown it is mainly confined within after neuronal uptake [8].

It is of note as well that one of the tau antibodies, 4E6, was associated with faster and more extensive clearance of FSB than 6B2 or control IgG1 (Fig. 4c). This acute efficacy difference is analogous to our recent report showing acute cognitive benefits of 4E6 whereas 6B2 was ineffective [10]. Here, as in that prior report, these benefits were not associated with extensive clearance of pathological tau as detected on Western blots. However, significant decrease was detected in soluble hyperphosphorylated tau in the 4E6 group compared to the 6B2 or IgG control groups following a single intravenous injection of 100 μg of antibody (about 3 mg/kg; Fig. 5d, f). That therapeutic effect is comparable to our prior study, in which a different tauopathy mouse model received three intraperitoneal injections of 4E6 or 6B2 (10 mg/kg) [10]. Hence, this type of two-photon approach analyzing antibody-mediated clearance of FSB in real time, allows for an efficient and sensitive in vivo screen of the therapeutic potential of tau antibodies. It is not surprising that it is more sensitive than western blot measurements because it entails direct analysis of live animals without the potentially confounding variables associated with the numerous steps involved in postmortem tissue processing for western blots. In addition, although we show here and previously that antibody-mediated tau clearance can be detected by staining with antibodies against various epitopes [2,4,15], some epitopes may be cleared better than others as shown here. This adds another variable to such analysis. In future studies, measurement of CSF tau levels in conjunction with two-photon imaging should further clarify target engagement of tau antibodies. Likewise, since FSB signal gradually fades with time (about 50% in two weeks), its injection prior to each imaging session may allow better detection of antibody efficacy. In addition, ELISA measurements of tau levels may be more sensitive than Western blot analyses and provide further insight into antibody-mediated tau clearance.

With the advantages of penetration into brain tissue and low phototoxicity, in vivo two-photon imaging is widely used in AD mouse models [30]. This includes to image neurites, dendritic spines, microglia, astrocytes, Aβ plaques, tau tangles and pre-tangles or neuronal and astrocytic activity. In particular, antibody therapies have been shown to clear Aβ plaques based on reduced signal from the fluorescent dye that labels Aβ [11]. Furthermore, camelid single-domain antibodies have been shown to cross the BBB and label Aβ deposits and neurofibrillary tau tangles in vivo using two-photon microcopy [31]. However, we are not aware of other two-photon studies showing antibody-mediated clearance of tau aggregates as we are reporting.

In summary, two-photon imaging provides a unique insight into the dynamics of uptake and clearance of mAbs, as well as the removal of their pathological targets in live animals. In addition to elucidating the mechanisms involved, this approach allows for an efficient in vivo assessment of the therapeutic potential of tau antibodies, and may be applied to related protein misfolding diseases, assuming that appropriate β-sheet dyes exist for those aggregates.

Acknowledgements

We thank Dr. Peter Davies (Albert Einstein College of Medicine and Long Island Jewish Medical Center) for the tau antibodies PHF1 and CP27.

Funding sources

This work was supported by the National Institutes of Health (NIH; AG032611, NS077239) and in part by NIH Sandy Recovery grants R24OD18340 and R24OD018339. The funding sources had no role in the writing of the manuscript or the decision to submit it for publication. No payment was received from a pharmaceutical company or other agency to write this article.

Declaration of interests

EMS is an inventor on patents on tau immunotherapy and related diagnostics that are assigned to New York University. Some of this technology is licensed to and is being co-developed with H. Lundbeck A/S.

Author contributions

Designing experiments: EMS, QW, JG. Performing experiments: QW, YL, JG. Analyzing data and writing manuscript: EMS, QW. All authors read and approved the final manuscript.

References

[1] Asuni AA, Quartermain D, Sigurdsson EM. Tau-based immunotherapy for dementia. Alzheimers Dement 2006;2:S40–1.
[2] Asuni AA, Boutajangout A, Quartermain D, Sigurdsson EM. Immunotherapy targeting pathological tau conformers in a tangle mouse model reduces brain pathology with associated functional improvements. J Neurosci 2007;27(34):9115–29.
[3] Boutajangout A, Ingadottir J, Davies P, Sigurdsson EM. Passive tau immunotherapy diminishes functional decline and clears tau aggregates in a mouse model of tauopathy. Alzheimers Dement 2010;6:S578 Suppl.
[4] Boutajangout A, Ingadottir J, Davies P, Sigurdsson EM. Passive immunization targeting pathological phospho-tau protein in a mouse model reduces functional decline and clears tau aggregates from the brain. J Neurochem 2011;118(4):658–67.
[5] Pedersen JT, Sigurdsson EM. Tau immunotherapy for Alzheimer's disease. Trends Mol Med 2015;21(6):394–402.
[6] Congdon EE, Sigurdsson EM. Tau-targeting therapies for Alzheimer disease. Nat Rev Neurol 2018;14:399–415.
[7] Congdon EE, Gu J, Sait HB, Sigurdsson EM. Antibody uptake into neurons occurs primarily via clathrin-dependent Fcgamma receptor endocytosis and is a prerequisite for acute tau protein clearance. J Biol Chem 2013;288(49):35452–65.
[8] Gu J, Congdon EE, Sigurdsson EM. Two novel Tau antibodies targeting the 396/404 region are primarily taken up by neurons and reduce Tau protein pathology. J Biol Chem 2013;288(46):33081–95.
[9] Krishnaswamy S, Lin Y, Rajamohamedsait WJ, Rajamohamedsait HB, Krishnamurthy P, Sigurdsson EM. Antibody-derived in vivo imaging of tau pathology. J Neurosci 2014;34(50):16835–50.
[10] Congdon EE, Lin Y, Rajamohamedsait HB, Shamir DB, Krishnaswamy S, Rajamohamedsait WJ, et al. Affinity of Tau antibodies for solubilized pathological Tau species but not their immunogen or insoluble Tau aggregates predicts in vivo and ex vivo efficacy. Mol Neurodegener 2016;11(1):62–85.
[11] Bacskai BJ, Kajdasz ST, Christie RH, Carter C, Games D, Seubert P, et al. Imaging of amyloid-beta deposits in brains of living mice permits direct observation of clearance of plaques with immunotherapy. Nat Med 2001;7(3):369–72.
[12] Velasco A, Fraser G, Delobel P, Ghetti B, Lavenir I, Goedert M. Detection of filamentous tau inclusions by the fluorescent Congo red derivative FSB [(trans,trans)-1-fluoro-2,5-bis(3-hydroxycarbonyl-4-hydroxy)styrylbenzene]. FEBS Lett 2008;582(6):901–6.
[13] Andorfer C, Kress Y, Espinoza M, de Silva R, Tucker KL, Barde YA, et al. Hyperphosphorylation and aggregation of tau in mice expressing normal human tau isoforms. J Neurochem 2003;86(3):582–90.
[14] Duff K, Eckman C, Zehr C, Yu X, Prada CM, Perez-Tur J, et al. Increased amyloid-beta42(43) in brains of mice expressing mutant presenilin 1. Nature 1996;383(6602):710–3.
[15] Boutajangout A, Quartermain D, Sigurdsson EM. Immunotherapy targeting pathological tau prevents cognitive decline in a new tangle mouse model. J Neurosci 2010;30(49):16559–66.
[16] Rajamohamedsait HB, Sigurdsson EM. Histological staining of amyloid and pre-amyloid peptides and proteins in mouse tissue. In: Sigurdsson EM, Calero M, Gasset M, editors. Amyloid Proteins. Methods in Molecular Biology (Methods and Protocols). , 2nd ed.New York: Humana Press; 2012. p. 411–24.
[17] Krishnaswamy S, Wu Q, Lin Y, Rajamohamedsait WJ, Rajamohamedsait HB, Sigurdsson EM. Tau antibody derivatives as diagnostic imaging ligands for tauopathies. Society for Neuroscience 46th annual meeting; 2016 San Diego, CA, USA. Abstract 199.09.
[18] Krishnamurthy PK, Deng Y, Sigurdsson EM. Mechanistic studies of antibody-mediated clearance of tau aggregates using an ex vivo brain slice model. Front Psych 2011;2:59.
[19] Collin L, Bohrmann B, Gopfert U, Oroszlan-Szovik K, Ozmen L, Gruninger F. Neuronal uptake of tau/pS422 antibody and reduced progression of tau pathology in a mouse model of Alzheimer's disease. Brain 2014;137:2834–46.
[20] Kondo A, Shahpasand K, Mannix R, Qiu J, Moncaster J, Chen CH, et al. Antibody against early driver of neurodegeneration cis P-tau blocks brain injury and tauopathy. Nature 2015;523(7561):431–6.
[21] Masliah E, Rockenstein E, Adame A, Alford M, Crews L, Hashimoto M, et al. Effects of alpha-synuclein immunization in a mouse model of Parkinson's disease. Neuron 2005;46(6):857–68.
[22] Tampellini D, Magrane J, Takahashi RH, Li F, Lin MT, Almeida CG, et al. Internalized antibodies to the Abeta domain of APP reduce neuronal Abeta and protect against synaptic alterations. J Biol Chem 2007;282(26):18895–906.
[23] Urushitani M, Ezzi SA, Julien JP. Therapeutic effects of immunization with mutant superoxide dismutase in mice models of amyotrophic lateral sclerosis. Proc Natl Acad Sci U S A 2007;104(7):2495–500.
[24] Gustafsson G, Eriksson F, Moller C, da Fonseca TL, Outeiro TF, Lannfelt L, et al. Cellular Uptake of alpha-Synuclein Oligomer-Selective Antibodies is Enhanced by the Extracellular Presence of alpha-Synuclein and Mediated via Fcgamma Receptors. Cell Mol Neurobiol 2017;37(1):121–31.
[25] Schon C, Hoffmann NA, Ochs SM, Burgold S, Filser S, Steinbach S, et al. Long-term in vivo imaging of fibrillar tau in the retina of P301S transgenic mice. PLoS One 2012;7(12):e53547.
[26] de Calignon A, Fox LM, Pitstick R, Carlson GA, Bacskai BJ, Spires-Jones TL, et al. Caspase activation precedes and leads to tangles. Nature 2010;464(7292):1201–4.
[27] D'Abramo C, Acker CM, Jimenez HT, Davies P. Tau passive immunotherapy in mutant P301L mice: antibody affinity versus specificity. PLoS One 2013;8(4):e62402.
[28] Yanamandra K, Kfoury N, Jiang H, Mahan TE, Ma S, Maloney SE, et al. Anti-tau antibodies that block tau aggregate seeding in vitro markedly decrease pathology and improve cognition in vivo. Neuron 2013;80(2):402–14.
[29] Castillo-Carranza DL, Sengupta U, Guerrero-Munoz MJ, Lasagna-Reeves CA, Gerson JE, Singh G, et al. Passive immunization with Tau oligomer monoclonal antibody reverses tauopathy phenotypes without affecting hyperphosphorylated neurofibrillary tangles. J Neurosci 2014;34(12):4260–72.
[30] Liebscher S, Meyer-Luehmann M. A peephole into the brain: neuropathological features of Alzheimer's disease revealed by in vivo two-photon imaging. Front Psych 2012;3:26.
[31] Li T, Vandesquille M, Koukouli F, Dudeffant C, Youssef I, Lenormand P, et al. Camelid single-domain antibodies: A versatile tool for in vivo imaging of extracellular and intracellular brain targets. J Control Release 2016;243:1–10.